Reentrant superconductivity in proximity to a topological insulator

T. Karabassov,[1] A. A. Golubov,[2,3] V. M. Silkin,[4,5,6] V. S. Stolyarov,[3,7] and A. S. Vasenko [1,8,*]

[1]*HSE University, 101000 Moscow, Russia*
[2]*Faculty of Science and Technology and MESA ^+ Institute for Nanotechnology, University of Twente, 7500 AE Enschede, The Netherlands*
[3]*Moscow Institute of Physics and Technology, 141700 Dolgoprudny, Russia*
[4]*Donostia International Physics Center (DIPC), Paseo Manuel de Lardizabal 4, San Sebastián/Donostia, 20018 Basque Country, Spain*
[5]*Departamento de Física de Materiales, Facultad de Ciencias Químicas, UPV/EHU, 20080 San Sebastián, Basque Country, Spain*
[6]*IKERBASQUE, Basque Foundation for Science, 48011 Bilbao, Spain*
[7]*Dukhov Research Institute of Automatics (VNIIA), 127055 Moscow, Russia*
[8]*I.E. Tamm Department of Theoretical Physics, P.N. Lebedev Physical Institute, Russian Academy of Sciences, 119991 Moscow, Russia*

Superconducting hybrid structures with topological order and induced magnetization offer a promising way to realize fault-tolerant quantum computation. However, the effect of the interplay between magnetization and the property of the topological insulator surface, otherwise known as spin-momentum locking on the superconducting proximity effect, still remains to be investigated. We relied on the quasiclassical self-consistent approach to consider the superconducting transition temperature in the two-dimensional superconductor/topological insulator (S/TI) junction with an in-plane helical magnetization on the TI surface. It has emerged that the presence of the helical magnetization leads to the nonmonotonic dependence of the critical temperature on the TI thickness for both cases when the magnetization evolves along or perpendicular to the interface. The results obtained can be helpful for designing novel superconducting nanodevices and better understanding the nature of superconductivity in S/TI systems with nonuniform magnetization.

I. INTRODUCTION

A leakage of the superconducting correlations into a magnetic material nearby [1–5] in superconductor/ferromagnet (S/F) heterostructures can be the reason for various effects emerging at the interface. For instance, the critical temperature T_c behaves nonmonotonically as a function of different system parameters in S/F bilayers with uniform magnetization [6] and multilayered S/F spin valves with a magnetization misalignment in F layers [7]. As it has been revealed theoretically by Fominov *et al.* in the S/F structures, under certain parameters T_c demonstrates reentrant behavior which originates from nontrivial dependence of a Cooper-pair wave function [6]. A similar effect can also result in oscillating Josephson critical current [8–14], density of states [15,16], and critical temperature [17–21] in S/F/S junctions.

Currently three-dimensional topological insulators (3D TI) pertain to a dramatically evolving area of condensed matter physics due to their potential application in superconducting nanoelectronics [22–27] and robust quantum computing [28,29]. There are special topologically protected states on the surface of the 3D TI that are protected from backscattering processes by the presence of strong spin-orbit coupling (SOC) and time-reversal symmetry (TRS) in such materials. These surface electrons possess spin-momentum locking properties, i.e., their spin and momentum directions are aligned

perpendicular to each other. Combination of a topological insulator and superconductor in a hybrid structure creates remarkable quantum properties [30]. For example, zero-energy Majorana modes can arise in these structures in the presence of an external magnetic field or a magnetic moment of an adjacent ferromagnet [31–38].

The proximity effect and symmetry properties of the superconducting correlations induced on the TI surface [38–42] as well as the impact of the effective magnetization presence in S/TI hybrids have been thoroughly studied [32,43]. There is currently a continuous concern for treating SOC effects in layered structures including S/TI systems in terms of the quasiclassical Green's functions [44–53]. Recently, the generalized quasiclassical theory was elaborated for a two-dimensional system with a strong SOC and exchange field [54]. Within the quasiclassical methods it has been found by Alidoust and Hamzehpour that a spontaneous supercurrent can flow in a Josephson junction where magnetized superconductors are weakly linked through the conducting surface of 3D TI [55].

According to the theory advanced by Zyuzin *et al.* in Ref. [56], there are no Josephson critical current oscillations in hybrid S/TI/S structures with a uniform in-plane field in the TI layer. At the same time, oscillations of the critical current are predicted in the junction where the TI surface with helical magnetization serves as a weak link. It is known that the presence of $0 - \pi$ phase transitions in the critical supercurrent may imply nontrivial critical temperature behavior and even the reentrance of T_c in the S/TI junction as in common S/F
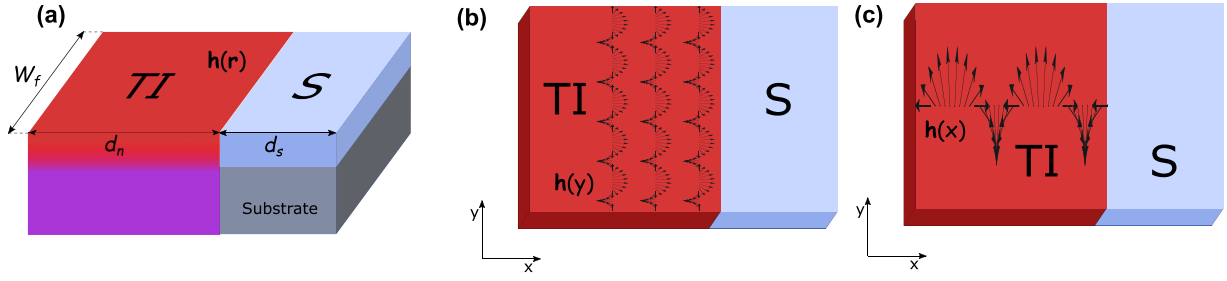
*avasenko@hse.ru

FIG. 1. (a) Schematic of a 3D topological insulator (TI)-superconductor (S) junction with a proximity-induced helical magnetization pattern. The magnetization vector is given by $\mathbf{h}(y) = h_0(\cos Qy, \sin Qy, 0)$ (b) and $\mathbf{h}(x) = h_0(\cos Qx, \sin Qx, 0)$ (c). The junction resides in the $x - y$ plane, and the S/TI interface lies in the y direction at $x = 0$. d_n and d_s are the thicknesses of TI and S layers, respectively, while W_f is the width of the junction.

bilayers [6,57,58]. Therefore the study of the T_c in the hybrids with both spin-orbit coupling and helical magnetization is essential for further understanding of superconductivity in the vicinity of the S/TI interface. Furthermore, the problem under consideration can be significant for engineering spin valves and other devices in superconducting nanoelectronics.

In the present work we aim to provide quantitative research of the critical temperature in the S/TI hybrid structure as a function of its parameters employing the quasiclassical Green's function approach. The helical magnetization pattern under consideration is similar to those previously studied in S/F bilayers with nonuniform spiral magnets [57–59]. Such hybrid systems consisting of superconducting layers and spiral magnets are important for spintronic applications, since reorientation of the spiral direction can be used as a method of spin-valve control [60–62]. However, the nature of the effects in the structure considered is different, since they are caused not only by an in-plane helical magnetization pattern but also by the spin-orbit coupling.

The paper is organized as follows. In Sec. II we discuss the theoretical model and basic equations for the cases when the helical magnetization evolves along or perpendicular to the S/TI interface. In Sec. III we present the results of the critical temperature calculations using the single-mode approximation. Finally, we point out concluding remarks in Sec. IV.

II. MODEL

In this work we consider the 2D nanostructure, which is depicted in the Fig. 1. It consists of superconductor S of thickness d_s and topological insulator (TI) of thickness d_n with proximity-induced helical magnetization patterns. The surface states of the TI layer are described by the Hamiltonian

$$\hat{H}(r) = \alpha(\hat{p} \times \hat{e}_z) \cdot \hat{\sigma} + \mathbf{h}(r) \cdot \hat{\sigma} - \mu. \tag{1}$$

Here α is the Fermi velocity, $\hat{p}$ is the momentum operator, $\hat{e}_z$ is the unity vector along the z axis, $\mathbf{h}(r)$ is the magnetization pattern, $\hat{\sigma}$ is a vector comprised of the Pauli matrices acting on the spin degree of freedom, and μ is the chemical potential in the system. We consider the following types of helical magnetization patterns:

$$\mathbf{h}(y) = h_0(\cos Qy, \sin Qy, 0), \tag{2}$$

$$\mathbf{h}(x) = h_0(\cos Qx, \sin Qx, 0), \tag{3}$$

where $Q = 2\pi/\lambda$, and λ determines the actual pattern of helical magnetization. It is important to note that we consider the variations of the magnetization $\mathbf{h}$ in the $x - y$ plane. Similar helical patterns with a period $\lambda \approx 10$ nm was observed experimentally in manganese on a tungsten substrate [63]. The orientation of the structure is along the x direction. In order to observe the inverse proximity effect, the superconductor must be two-dimensional. Such disordered homogeneous superconducting 2D films can be obtained with the help of modern deposition techniques [64].

To calculate the critical temperature $T_c(d_n)$ of this structure, we assume the diffusive limit, when the elastic scattering length ℓ is much smaller than the coherence length [65], and use the framework of the linearized Usadel equations for the S and TI layers in Matsubara representation [66,67]. We perform the calculations in the low-proximity limit, expanding the Green's function around the bulk solution,

$$\hat{g} = \begin{pmatrix} \mathrm{sgn}\omega_n & f \\ -f^* & -\mathrm{sgn}\omega_n \end{pmatrix}, \tag{4}$$

where f^* is the complex conjugation of the function f. Such a limit is experimentally feasible and can be easily achieved in the vicinity of the superconducting critical temperature T_c or in a hybrid structure with low transparent interfaces.

A. Helical magnetization h(y)

In this section we establish the equations for the magnetization pattern evolving along the S/TI interface indicated in Eq. (2), i.e., in y direction. Since the low-proximity limit is assumed, near T_c the normal Green's function in a superconductor is $g_s = \mathrm{sgn}\omega_n$, and the Usadel equation for the anomalous Green's function f_s takes the following form. In the S layers ($0 < x < d_s$) it reads

$$\xi_s^2 \pi T_{cs} \left(\frac{\partial^2}{\partial x^2} + \frac{\partial^2}{\partial y^2} \right) f_s - |\omega_n| f_s + \Delta = 0. \tag{5}$$

In the TI layer we consider the Usadel equation derived in Ref. [56], where f_T is the anomalous Green's function in the TI layer,

$$\left(\frac{\partial}{\partial x} - \frac{2i}{\alpha} h_y(y) \right)^2 f_T + \left(\frac{\partial}{\partial y} + \frac{2i}{\alpha} h_x(y) \right)^2 f_T = \frac{|\omega_n|}{\xi_n^2 \pi T_{cs}} f_T. \tag{6}$$

Since we consider the dirty limit, the spinless Green's function matrix $\hat{g}_s$ is used in our calculations, whereas the spin texture is contained in the matrix $\check{g}(\mathbf{n}_F) = \hat{g}(1 + \hat{\eta} \cdot \mathbf{n}_F)/2$, where $\mathbf{n}_F = \mathbf{p}_F/p_F$, $\hat{\eta} = (-\sigma_2, \sigma_1)$, and σ_i are the Pauli matrices. The spin-momentum locking effect can be seen from the spin matrix $\check{g}$, so that spin and momentum are always fixed at the right angle. Finally, the self-consistency equation reads [66]

$$\Delta \ln \frac{T_{cs}}{T} = \pi T \sum_{\omega_n} \left(\frac{\Delta}{|\omega_n|} - f_s \right). \tag{7}$$

In Eqs. (5)–(7) $\xi_s = \sqrt{D_s/2\pi T_{cs}}$, $\xi_n = \sqrt{D_n/2\pi T_{cs}}$, $\omega_n = 2\pi T(n + \frac{1}{2})$, where $n = 0, \pm 1, \pm 2, \ldots$ are the Matsubara frequencies, T_{cs} is the critical temperature of the superconductor S, and $f_{s(T)}$ denotes the singlet components of the anomalous Green's function in the S(TI) region (we assume $\hbar = k_B = 1$).

As long as our 2D system is periodic in y direction and large values of the helical magnetization parameter Q are considered such that $\lambda \ll W_f$, we can expand the anomalous Green's functions using the Fourier series. The function f_T can then be written as

$$f_T(x, y) = \sum_{p=-\infty}^{+\infty} f_T^{(p)}(x) e^{ipQy}. \tag{8}$$

The Usadel equation in the TI layer for the amplitudes $f_T^{(p)}$ then takes the following form:

$$\left(\frac{\partial}{\partial x} - \frac{2i}{\alpha} h_y(y) \right)^2 f_T^{(p)} - p^2 Q^2 f_T^{(p)} - \frac{4pQh_x(y)}{\alpha} f_T^{(p)}$$
$$= \left(\frac{|\omega_n|}{\xi_n^2 \pi T_{cs}} + \frac{4h_x^2(y)}{\alpha^2} - \frac{2ih_x'(y)}{\alpha} \right) f_T^{(p)}, \tag{9}$$

where $h_x'(y)$ is a derivative of h_x along the y direction. In the S layer the singlet function f_s as well as Δ can be also expanded into the Fourier series,

$$f_s(x, y) = \sum_{p=-\infty}^{+\infty} f_s^{(p)}(x) e^{ipQy}, \tag{10}$$

$$\Delta(x, y) = \sum_{p=-\infty}^{+\infty} \Delta^{(p)}(x) e^{ipQy}. \tag{11}$$

The amplitudes $f_s^{(p)}$ obey the following equation:

$$\xi_s^2 \left(\frac{\partial^2 f_s^{(p)}}{\partial x^2} - p^2 Q^2 f_s^{(p)} - \frac{|\omega_n|}{\xi_s^2 \pi T_{cs}} f_s^{(p)} \right) + \frac{\Delta^{(p)}}{\pi T_{cs}} = 0. \tag{12}$$

The self-consistency equation for the Fourier amplitudes in the superconductor can be written as

$$\Delta^{(p)} \ln \frac{T_{cs}}{T} = \pi T \sum_{\omega_n} \left(\frac{\Delta^{(p)}}{|\omega_n|} - f_s^{(p)} \right). \tag{13}$$

From the equations above, it is clear that the amplitudes of the Fourier series are decoupled in the vicinity of the critical temperature. Therefore each Fourier component p satisfies certain Usadel equations and the boundary conditions. Moreover, every single Fourier harmonic p of the anomalous Green's function $f_s^{(p)}$ and pair amplitude $\Delta^{(p)}$ determines particular T_c through the corresponding gap equation. However,

the physical solution is the one which gives the highest critical temperature T_c, i.e., the solution is energetically favorable.

We also need to supplement the equations above with proper boundary conditions to solve the problem [56,68]. We assume a low transparency limit of the interface between the topological insulator (TI) and superconducting layer (S). It is also assumed that spin is conserved when the electrons tunnel across the interface, whereas momentum is not conserved. For the Fourier harmonics of the solution $f^{(p)}$ that we have introduced above and taking all the simple transformations into account, the boundary conditions at $x = 0$ take the form

$$\gamma_B \xi_n \left(\frac{\partial}{\partial x} - \frac{2ih_y(y)}{\alpha} \right) f_T(0) = f_s(0) - f_T(0), \tag{14}$$

$$\gamma \xi_n \left(\frac{\partial}{\partial x} - \frac{2ih_y(y)}{\alpha} \right) f_T(0) = \xi_s \frac{\partial f_s(0)}{\partial x}. \tag{15}$$

Here we omitted the component index p. The parameter $\gamma_B = R_b \sigma_n / \xi_n$ is the transparency parameter, which is the ratio of resistance per unit area of the surface of the tunneling barrier to the resistivity of the TI layer and describes the effect of the interface barrier [68,69]. In (15) the dimensionless parameter $\gamma = \xi_s \sigma_n / \xi_n \sigma_s$ determines the strength of suppression of superconductivity in the S layers near the S/TI interface compared to the bulk (inverse proximity effect). No suppression occurs for $\gamma = 0$, while strong suppression takes place for $\gamma \ll 1$. Here $\sigma_{s(n)}$ is the normal-state conductivity of the S(TI) layer.

These boundary conditions should also be supplemented with vacuum conditions at the edges ($x = -d_n$ and $x = +d_s$),

$$\frac{\partial f_s(d_s)}{\partial x} = 0, \quad \left(\frac{\partial}{\partial x} - \frac{2ih_y(y)}{\alpha} \right) f_T(-d_n) = 0. \tag{16}$$

The solution of Eq. (9) can be found in the form

$$f_T^{(p)} = C(\omega_n) \cosh[\kappa_{p,y}(x + d_n)] \exp\left[\frac{2ih_y(y)}{\alpha}(x + d_n) \right], \tag{17}$$

where

$$k_{p,y} = \sqrt{ \frac{|\omega_n|}{\xi_n^2 \pi T_{cs}} + \frac{4}{\alpha^2} h_x^2(y) - \frac{2ih_x'(y)}{\alpha} + Q_p },$$

$$Q_p = p^2 Q^2 + \frac{4pQh_x(y)}{\alpha}. \tag{18}$$

Here $C(\omega_n)$ is a coefficient found from the boundary conditions, and the wave vector acquires an additional imaginary term due to fast oscillations of the anomalous Green's function along the y direction compared to the case of uniform magnetization ($Q = 0$). The introduced solution to the equation automatically satisfies the vacuum boundary conditions (16).

As long as Δ is assumed to be real valued function, we write our equations for the anomalous Green's functions in the real form. Also, we consider only positive Matsubara frequencies ω_n. Following the standard procedure we obtain a final set of equations sufficient to calculate the critical temperature as a function of d_n.

Using the boundary conditions (14) and (15), we would like to write the problem in a closed form with respect to the Green's function f_s. At $x = 0$ the boundary conditions can be

written as

$$\xi_s \frac{\partial f_s(0)}{\partial x} = \frac{\gamma}{\gamma_b + A_{pT}(\omega_n)} f_s(0), \tag{19}$$

where

$$A_{pT}(\omega_n) = \frac{1}{k_{p,y}} \coth(k_{p,y} d_n).$$

The boundary condition (19) is complex. In order to rewrite it in the real form, we use the following relation:

$$f^{\pm} = f(\omega_n) \pm f(-\omega_n). \tag{20}$$

According to the Usadel equation (5), there is a symmetry relation $f(-\omega_n) = f^*(\omega_n)$ which implies that f^+ is a real while f^- is a purely imaginary function. Then we rewrite the Usadel equation in the S layer in terms of f_s^+ and f_s^- utilizing symmetry relation (20). Since the pair potential Δ is considered to be real valued function, we can find the solution analytically in the Usadel equation for the imaginary function f_s^-. Using the solution found analytically, it is possible to derive the complex boundary condition (19) in the real form for the function f_s^+,

$$\xi_s \frac{\partial f_s^+(0)}{\partial x} = W^{(p)}(\omega_n) f_s^+(0), \tag{21}$$

where we used the notations

$$W^{(p)}(\omega_n) = \gamma \frac{A_{ps}(\gamma_b + \mathrm{Re}A_{pT}) + \gamma}{A_{ps}|\gamma_b + A_{pT}|^2 + \gamma(\gamma_b + \mathrm{Re}A_{pT})},$$

$$A_{ps} = \kappa_{ps} \tanh(\kappa_{ps} d_s), \quad \kappa_{ps} = \sqrt{Q^2 p^2 + \frac{|\omega_n|}{\xi_s^2 \pi T_{cs}}},$$

$$A_{pT}(\omega_n) = \frac{1}{k_{p,y}} \coth(k_{p,y} d_n). \tag{22}$$

In the same way we rewrite the self-consistency equation for Δ in terms of the symmetric function f_s^+ considering only positive Matsubara frequencies,

$$\Delta^{(p)} \ln \frac{T_{cs}}{T} = \pi T \sum_{\omega_n > 0} \left(\frac{2\Delta^{(p)}}{\omega_n} - f_s^{(p)+} \right), \tag{23}$$

as well as the Usadel equation in the superconducting layer,

$$\xi_s^2 \left(\frac{\partial^2 f_s^{(p)+}}{\partial x^2} - \kappa_{ps}^2 f_s^{(p)+} \right) + \frac{2\Delta^{(p)}}{\pi T_{cs}} = 0. \tag{24}$$

To calculate the critical temperature in the considered system, we use Eqs. (21)–(24), together with the vacuum boundary condition (16) for the Fourier components $f_s^{(p)+}$.

B. Helical magnetization h(x)

Here we consider the system consisting of a superconductor and topological insulator with helical magnetization pattern presented in Eq. (3). In this case the Usadel equation should be rewritten in terms of magnetization $\mathbf{h}(x)$. We assume that the anomalous Green's function does not depend on the y coordinate, and thus the corresponding derivatives are neglected. The Usadel equation in the TI layer then takes the

following form:

$$\left(\frac{\partial}{\partial x} - \frac{2ih_y(x)}{\alpha} \right)^2 f_T - \frac{4h_x^2(x)}{\alpha^2} f_T = \frac{|\omega_n|}{\xi_n^2 \pi T_{cs}} f_T. \tag{25}$$

In order to rewrite Eq. (25) in real form we introduce the following ansatz:

$$f_T(x) = f_L(x) \exp \left[-i \frac{2h_0}{\alpha Q} \cos Qx \right]. \tag{26}$$

Inserting this substitution into Eq. (25), we obtain an equation for the real valued function in the TI layer,

$$\frac{\partial^2 f_L}{\partial x^2} = \left(\frac{|\omega_n|}{\xi_n^2 \pi T_{cs}} + \frac{4h_0^2 \cos^2 Qx}{\alpha^2} \right) f_L. \tag{27}$$

For this system we utilize the same boundary conditions as in the previous section and express them in the real form using the symmetry relation (20). After the substitutions the boundary conditions take the form

$$\gamma_B \xi_n \frac{\partial f_L(0)}{\partial x} = C_0 f_s^+(0) - f_L(0), \tag{28}$$

$$\gamma \xi_n \frac{\partial f_L(0)}{\partial x} = \xi_s C_0 \frac{\partial f_s^+(0)}{\partial x}, \tag{29}$$

where $C_0 = \cos(2h_0/\alpha Q)$. Finally, the boundary conditions at the free edges at $x = d_s$ and $x = -d_n$ are

$$\frac{\partial f_s(d_s)}{\partial x} = 0, \quad \frac{\partial f_L(-d_n)}{\partial x} = 0. \tag{30}$$

Similarly, we introduce the self-consistency equation for Δ in terms of the symmetric function f_s^+, treating only positive Matsubara frequencies,

$$\Delta \ln \frac{T_{cs}}{T} = \pi T \sum_{\omega_n > 0} \left(\frac{2\Delta}{\omega_n} - f_s^+ \right), \tag{31}$$

and the Usadel equation in the S layer,

$$\xi_s^2 \pi T_{cs} \frac{\partial^2 f_s^+}{\partial x^2} - \omega_n f_s^+ + 2\Delta = 0. \tag{32}$$

Since Eq. (25) cannot be solved analytically, to obtain the critical temperature T_c the whole set of equations (27)–(32) must be calculated numerically.

C. Single-mode approximation

In this section we present the single-mode approximation method. The solution of the problems (21)–(24) and (27)–(32) can be searched in the form of the following ansatz:

$$f_s^+(x, \omega_n) = f(\omega_n) \cos \left(\Omega \frac{x - d_s}{\xi_s} \right), \tag{33a}$$

$$\Delta(x) = \delta \cos \left(\Omega \frac{x - d_s}{\xi_s} \right), \tag{33b}$$

where δ and Ω do not depend on ω_n. The above solution automatically satisfies the boundary condition (16) at $x = d_s$.
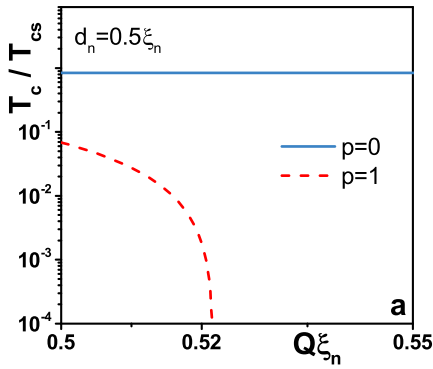
FIG. 2. $T_c(Q)$ dependencies for two harmonic solutions at $\xi_n h_0/\alpha = 0.1$. The behavior realized physically is the one which gives the highest T_c. The parameters used in the calculations: $\gamma_B = 0.1$, $W_f = 100\xi_n$.

1. Case of **h(y)**

Substituting the expression (33) into (24) we obtain

$$f(\omega_n) = \frac{2\delta}{\Omega^2 \pi T_{cs} + \pi T_{cs}\xi_s^2 Q^2 p^2}. \qquad (34)$$

To determine the critical temperature T_c we have to substitute Eqs. (33) and (34) into the self-consistency equation (23) at $T = T_c$. Then it is possible to rewrite the self-consistency equation in the following form:

$$\ln \frac{T_{cs}}{T_c} = \psi\left(\frac{1}{2} + \frac{\Omega^2 + Q^2 p^2}{2}\frac{T_{cs}}{T_c}\right) - \psi\left(\frac{1}{2}\right), \qquad (35)$$

where ψ is the digamma function,

$$\psi(z) \equiv \frac{d}{dz}\ln\Gamma(z), \quad \Gamma(z) = \int_0^\infty \eta^{z-1}e^{-\eta}d\eta. \qquad (36)$$

Boundary condition (21) at $x = 0$ yields the following equation for Ω:

$$\Omega \tan\left(\Omega\frac{d_s}{\xi_s}\right) = W^{(p)}(\omega_n). \qquad (37)$$

Generally, in order to calculate the critical temperature T_c, the problem is put on the grid with finite number of the Fourier harmonics N and the following condition should be used:

$$T_c = \max\left(T_c^{(p)}\right) \quad p = 0, 1, 2...N. \qquad (38)$$

The critical temperature behavior is found from the solution of the transcendental equations (35) and (37), as well as Eq. (38). Thus the solution that gives the highest critical temperature T_c is the only one which is realized physically. However, we find that to calculate the critical temperature it is sufficient to use the zeroth ($p = 0$) harmonic of the full Fourier solution for a wide parameter range. In Fig. 2 we demonstrate the situation when the T_c calculation requires consideration of only the $p = 0$ Fourier component. It is possible due to rapid decay of the $p > 0$ components of the solution as functions of Q. From the figure it can be seen that for $Q\xi_n > 0.5$ the critical temperature for $p = 1$ is not only lower than T_c for $p = 0$ but rapidly drops to zero at $Q\xi_n \approx 0.52$.

Such behavior of the components with $p > 0$ allows us to calculate the critical temperature by taking the appropriately large Q, when the $p = 0$ harmonic is sufficient for the T_c calculation of the S/TI bilayer. Since in this case the function $T_c(y)$ quickly oscillates ($Q\xi_n \gg 1$), we also perform the averaging of the critical temperature along the y direction.

2. Case of **h(x)**

Since the solution of Eq. (27) cannot be found in analytical form, we calculate the function f_L numerically and solve the problem of Eqs. (27)–(32) in the single-mode approximation (33).

III. RESULTS AND DISCUSSION

In this section we present the results of the critical temperature calculations using the single-mode approximation. Some of the parameters are set to the certain values and are not changed throughout the paper, otherwise it is indicated. Such parameters are $\gamma = 0.2$, $\xi_s = \xi_n$ and the width of the junction $W_f = 20\xi_n$.

A. Case of **h(y)**

In Fig. 3(a) the critical temperature dependencies are plotted for different values of the transparency parameter γ_B. The helical magnetization parameter $\xi_n h_0/\alpha = 0.25$ and $\lambda = \xi_n$ ($\lambda = 2\pi/Q$). We normalize T_c by its maximum value T_{cs} in the absence of the proximitized TI layer and the TI thickness d_n by the coherence length ξ_n. As expected, for a perfectly transparent S/TI interface (blue solid line) the critical temperature decreases significantly, showing nonmonotonic behavior with a minimum at $d_n \approx \xi_n$, and eventually saturates at $T_c \approx 0.15T_{cs}$. For larger values of γ_B or at moderate and high resistances of the interface, $T_c(d_n)$ saturates at larger temperatures and the position of the T_c minimum shifts towards smaller values of d_n. Unlike $T_c(d_n)$ dependencies in ordinary S/F systems with uniform as well as out-of-plane spiral magnetization, here the critical temperature does not demonstrate completely reentrant behavior, i.e., T_c does not vanish in a certain interval of d_n.

The impact of different λ on the critical temperature behavior is depicted in Fig. 3(b). Here we took $\gamma_B = 0.1$, $\xi_n h_0/\alpha = 0.25$, and $d_s = 1.2\xi_s$. From the plot one can notice that T_c becomes more suppressed for smaller values of spatial period λ (which is expressed in terms of Q as $\lambda = 2\pi/Q$), which means that λ acts as an additional cause of the superconducting correlation depairing. It is worth mentioning that a rather opposite effect has been observed in the S/F hybrid bilayers with out-of-plane spiral magnetization [58], where T_c experienced enhancement as Q increased.

B. Uniform and helical magnetizations

In this section we compare the $T_c(d_n)$ behavior in S/TI bilayers with the uniform and helical magnetization induced on the TI surface. In Fig. 4 the comparison between S/TI with uniform **h** and with **h(y)** is shown. From the figure one can see that there is a significant difference in the $T_c(d_n)$ dependence for both cases. First, let us discuss the origin of the T_c
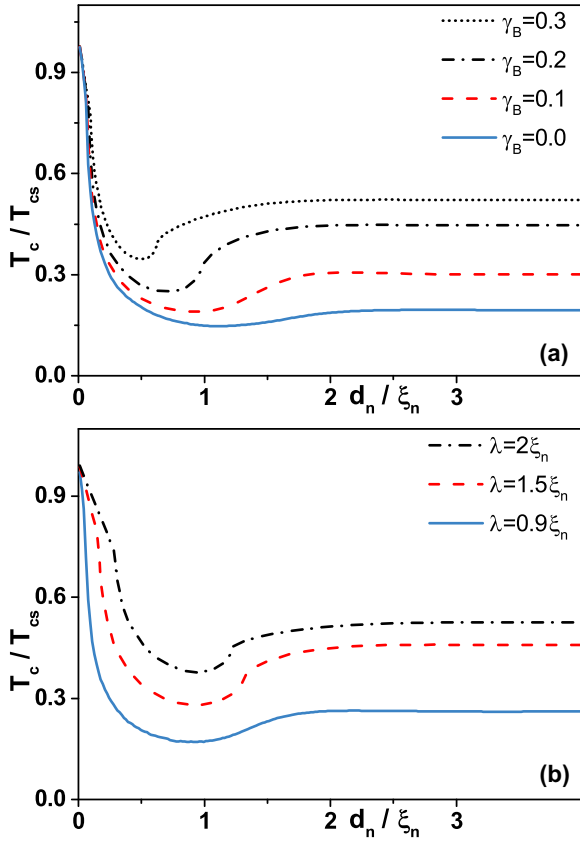
FIG. 3. The behavior of the critical temperature T_c as a function of d_n. (a) Each plot corresponds to particular value of the transparency parameter γ_B: blue solid line to $\gamma_B = 0$, red dashed line to $\gamma_B = 0.1$, black dash-dotted line to $\gamma_B = 0.2$, and dotted line to $\gamma_B = 0.3$. (b) Effect of λ on $T_c(d_n)$ dependence. Each curve corresponds to a particular value of λ: blue solid line to $\lambda = 0.9\xi_n$, red dashed line to $\lambda = 1.5\xi_n$, and black dash-dotted line to $\lambda = 2\xi_n$. The parameters used in the calculations: $\xi_n h_0/\alpha = 0.25$, $Q = 2\pi/\lambda$, $\lambda = \xi_n$ (for plot a), $d_s = 1.2\xi_s$.

suppression in the case of a uniformly magnetized TI surface. The wave vector of the pair correlations in the topological insulator can be written as

$$\kappa_0 = \sqrt{\frac{2\omega_n}{D} + \frac{4}{\alpha^2} h_x^2}, \tag{39}$$

where h_x is the magnetization component along the x direction. Here h_x is responsible for depairing of the superconducting correlations and suppresses the critical temperature T_c with the decay length $\xi = 1/\kappa \approx \min[\sqrt{2\omega_n/D}, \alpha/2h_x]$. However, the h_y component of the magnetization does not play a role in the suppression of superconducting correlations but introduces a phase shift in the wave function, which has no quantitative effect on T_c. Thus, in Fig. 4 the critical temperature in the case of uniform magnetization (red solid lines) expresses monotonic decay due to the h_x component.

Other types of behavior appear when large enough values of Q are considered in the system. In this case the wave vector acquires additional imaginary terms of the form (18) and for
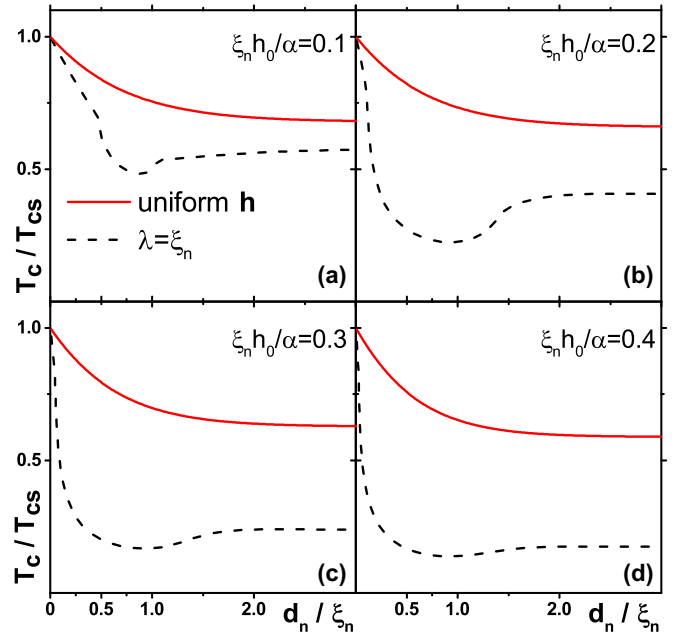

FIG. 4. Comparison of the critical temperature behavior between the S/TI bilayer with uniform magnetization and S/TI bilayer with helical magnetization pattern introduced in Eq. (2). The curves were calculated for different values of h_0/α: plot (a) corresponds to $\xi_n h_0/\alpha = 0.1$, plot (b) to $\xi_n h_0/\alpha = 0.2$, plot (c) to $\xi_n h_0/\alpha = 0.3$, and plot (d) to $\xi_n h_0/\alpha = 0.4$. The parameters γ and the coherence lengths are set to the identical values mentioned above. The transparency parameter for both systems $\gamma_B = 0.1$.

the zeroth harmonic ($p = 0$) can be written as

$$k_{0,y} = \sqrt{\frac{|\omega_n|}{\xi_n^2 \pi T_{cs}} + \frac{4h_0^2}{\alpha^2} \cos^2 Qy + \frac{2iQh_0}{\alpha} \sin Qy}. \tag{40}$$

Now the decay length becomes inverse proportional to $\sqrt{Q}$ for sufficiently large Q, as $\xi = 1/\kappa \approx \min[\sqrt{2\omega_n/D}, \alpha/2h_0, \sqrt{\alpha/2h_0Q}]$.

In fact, the critical temperature T_c demonstrates nonmonotonic behavior due to fast oscillations of helical magnetization along the y axis. This behavior is indicated by black dashed lines (Fig. 4), and it can be seen that $T_c(d_n)$ loses its nonmonotonicity as h_0/ξ_n grows from clearly pronounced (plots a and b) to hardly recognizable minimum (plots c and d) in the dependence.

C. Case of **h(x)**

Now we turn to the case of an S/TI hybrid structure with the TI layer magnetized along the x axis [Fig. 1(c)]. In Fig. 5 the critical temperature dependencies as functions of the TI layer thickness d_n are shown. The effect of varying magnetization strength h_0 with the parameter Q fixed to $Q = 2.0$ is shown in the upper plot [Fig. 5(a)]. From the plot we can distinguish three types of T_c behavior. For small values of h_0/α the critical temperature demonstrates slightly nonmonotonic behavior with a kink at $d_n \approx \xi_n$ and eventual saturation (a black dotted line). This nonmonotonic feature becomes more pronounced as h_0/α is increased (a blue solid line). However, for certain values of magnetization strength h_0 the critical
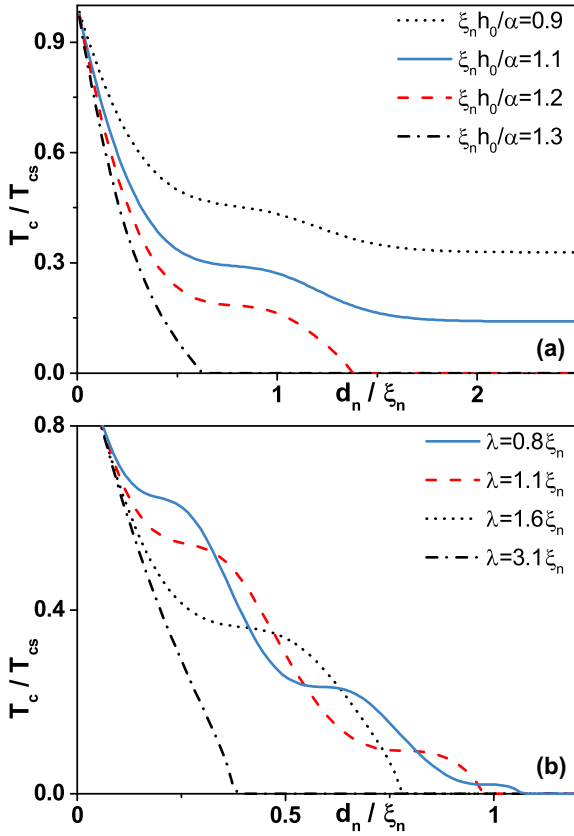
FIG. 5. The $T_c(d_n)$ dependencies for the configuration of helical magnetization introduced in Eq. (3). (a) Each curve corresponds to a particular value of h_0/α with fixed helical magnetization parameter $Q = 2$. Black dotted line corresponds to $\xi_n h_0/\alpha = 0.9$, blue solid line to $\xi_n h_0/\alpha = 1.1$, red dashed line to $\xi_n h_0/\alpha = 1.2$, and black dash-dotted line to $\xi_n h_0/\alpha = 1.3$. (b) The dependencies correspond to certain values of λ and fixed $\xi_n h_0/\alpha = 1.4$. Blue solid line $\lambda = 0.8\xi_n$, red dashed line $\lambda = 1.1\xi_n$, black dotted line $\lambda = 1.6\xi_n$, and dash-dotted line $\lambda = 3.1\xi_n$. The rest of the parameters used in the calculations are $\gamma_B = 0$, $d_s = 1.2\xi_s$.

FIG. 6. Influence of the arbitrary initial phase ϕ_0 in the magnetization pattern $\mathbf{h}(x) = h_0[\cos(Qx + \phi_0), \sin(Qx + \phi_0), 0]$. Each curve corresponds to a particular value of ϕ_0: red dotted line to $\phi_0 = 0$, blue solid line to $\phi_0 = \pi/4$, and black dashed line to $\phi_0 = \pi/2$. (a) $T_c(d_n)$ dependencies calculated for $\xi_n h_0/\alpha = 1.4$ and $\lambda = \xi_n$. The inset plot shows T_c behavior as a function of phase ϕ_0 for fixed thickness $d_n = 2\xi_n$ and two different values of $\xi_n h_0/\alpha = 1, 1.4$. (b) $T_c(Q)$ curves calculated for $d_n = \xi_n$ and $\xi_n h_0/\alpha = 1.2$. The parameters used in the calculations are $\gamma_B = 0$, $\xi_n h_0/\alpha = 0.25$, and $d_s = 1.2\xi_s$.

temperature drops to zero gradually (a red dashed line). Finally, at relatively large h_0 the critical temperature drops sharply down to zero without any bend (a black dash-dotted line).

The origin of such $T_c(d_n)$ curves is a coupling of helical magnetization and momentum of the quasiparticles. However, unlike the magnetization pattern $h(y)$, here the topological insulator TI is magnetized by $h(x)$ along the direction of d_n. Hence the effects on the critical temperature are more explicit and clearer to understand. As it was discussed above, the h_y component has no quantitative impact on the magnitude of T_c; therefore, the observed effects are purely due to variation of h_x and, namely, because of its periodicity. Obviously, the number of kinks demonstrated in Fig. 5(a), where we observed just one, depends on magnetization parameter $Q = 2\pi/\lambda$. In Fig. 5(b) the critical temperature behavior for different Q is shown. It can be seen that the smaller the spatial magnetization period λ, the more kinks are produced in the T_c.

In the calculations above we assumed that the magnetization pattern $\mathbf{h}(x)$ at $x = 0$ reduces to $\mathbf{h}(0) = h_0(1, 0, 0)$, which
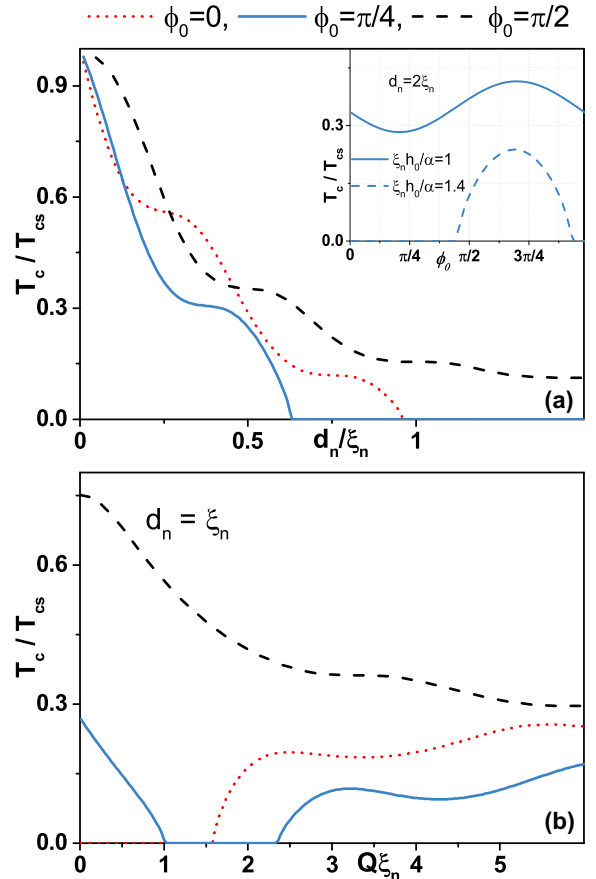
implies that the initial "phase" is 0. In practice, it may be possible to have an arbitrary initial phase in the experimental samples. It is very important to consider such a possibility, since T_c decays significantly in our system as a function of the TI thickness d_n. We can take into account ϕ_0 simply by rewriting the magnetization pattern (3) as

$$\mathbf{h}(x) = h_0[\cos(Qx + \phi_0), \sin(Qx + \phi_0), 0]. \quad (41)$$

In Fig. 6(a) the effect of various initial ϕ_0 on $T_c(d_n)$ for fixed $h_0/\alpha = 1.4$ and $\lambda = \xi_n$ is illustrated. From the plot we observe that while $\phi_0 = 0$ and $\phi_0 = \pi/4$ contribute to faster decay of T_c as a function of d_n (red dotted and blue solid line), the critical temperature has higher values at almost every d_n for $\phi_0 = \pi/2$ (black dashed line). The inset shows T_c as a function of ϕ_0 for fixed $d_n = 2\xi_n$.

Another interesting result can be noticed in Fig. 6(b) illustrating $T_c(Q)$ dependencies for the same values of ϕ_0 and fixed TI layer thickness $d_n = \xi_n$. One can recognize that depending on ϕ_0 the critical temperature behaves differ-

ently as Q changes. For $\phi_0 = 0$ (red dotted line) there is no superconductivity in the $Q\xi_n$ interval $[0, 1.5]$, since T_c is completely suppressed by slowly evolving near extremum h_x magnetization component at the vicinity of the S/TI interface. However, for $\phi_0 = \pi/4$ (blue solid line) T_c decays rapidly and vanishes at $Q\xi_n \approx 1$ but eventually restores at $Q\xi_n \approx 2.4$. Finally, in the case of $\phi_0 = \pi/2$ (black dashed line) the critical temperature is almost not suppressed at small values of Q but decays gradually as Q is further increased.

IV. CONCLUSION

In this work we have formulated a theoretical approach and presented the results of a quantitative investigation of the superconducting critical temperature in the S/TI hybrid structure where an in-plane helical magnetization is induced at the TI surface. The calculations are based on the quasiclassical Usadel equations, taking into account spin-orbit coupling at the surface of the topological insulator. We have assumed superconducting *s*-wave pairing symmetry in our calculations. which is justified in the dirty limit. The reason is that in the diffusive regime all anisotropic components of the superconducting order parameter are fully suppressed.

We have found that in the case of in-plane helical magnetization $\mathbf{h}(y)$ evolving along the interface, the calculations reveal nonmonotonic behavior of the critical temperature as a function of the TI layer thickness with a well-pronounced minimum, the effect of which is absent in the case of uniform magnetization. Despite the fact that in conventional S/F bilayers with out-of-plane spiral magnetization quite similar behavior of T_c as a function of the F layer thickness d_n has been observed, we find rather opposite critical temperature behavior depending on the magnetization parameter Q. The question of $T_c(d_n)$ behavior in the exact same configuration without SOC, i.e., in 2D S/F bilayers with an in-plane rotating magnetization, requires separate investigation.

In the case of helical magnetization evolving perpendicular to the interface $\mathbf{h}(x)$, the critical temperature demonstrates highly nonmonotonic behavior as well. However, this dependence has been shown to be qualitatively different from the case of $\mathbf{h}(y)$, showing the number of kinks, which depends on helical magnetization parameters. The results are important for further understanding of the underlying physics and potential future applications of superconductor-TI hybrid systems.

[1] E. A. Demler, G. B. Arnold, and M. R. Beasley, Phys. Rev. B **55**, 15174 (1997).

[2] A. Ozaeta, A. S. Vasenko, F. W. J. Hekking, and F. S. Bergeret, Phys. Rev. B **86**, 060509(R) (2012).

[3] F. S. Bergeret and I. V. Tokatly, Phys. Rev. Lett. **110**, 117003 (2013).

[4] F. S. Bergeret, A. F. Volkov, and K. B. Efetov, Rev. Mod. Phys. **77**, 1321 (2005).

[5] A. I. Buzdin, Rev. Mod. Phys. **77**, 935 (2005).

[6] Y. V. Fominov, N. M. Chtchelkatchev, and A. A. Golubov, Phys. Rev. B **66**, 014507 (2002).

[7] Ya. V. Fominov, A. A. Golubov, T. Yu. Karminskaya, M. Yu. Kupriyanov, R. G. Deminov, and L. R. Tagirov, JETP Lett. **91**, 308 (2010) [Pis'ma ZhETF **91**, 329 (2010)].

[8] A. I. Buzdin, L. N. Bulaevskii, and S. V. Panyukov, Pis'ma Zh. Eksp. Teor. Fiz. **35**, 147 (1982) [JETP Lett. **35**, 178 (1982)].

[9] A. I. Buzdin and M. Yu. Kupriyanov, Pis'ma Zh. Eksp. Teor. Fiz. **53**, 308 (1991) [JETP Lett. **53**, 321 (1991)].

[10] V. V. Ryazanov, V. A. Oboznov, A. Yu. Rusanov, A. V. Veretennikov, A. A. Golubov, and J. Aarts, Phys. Rev. Lett. **86**, 2427 (2001).

[11] V. A. Oboznov, V. V. Bol'ginov, A. K. Feofanov, V. V. Ryazanov, and A. I. Buzdin, Phys. Rev. Lett. **96**, 197003 (2006).

[12] A. V. Vedyayev, N. V. Ryzhanova, and N. G. Pugach, J. Magn. Magn. Mat. **305**, 53 (2006).

[13] A. S. Vasenko, A. A. Golubov, M. Yu. Kupriyanov, and M. Weides, Phys. Rev. B **77**, 134507 (2008).

[14] S. V. Bakurskiy, V. I. Filippov, V. I. Ruzhickiy, N. V. Klenov, I. I. Soloviev, M. Yu. Kupriyanov, and A. A. Golubov, Phys. Rev. B **95**, 094522 (2017).

[15] T. Kontos, M. Aprili, J. Lesueur, and X. Grison, Phys. Rev. Lett. **86**, 304 (2001).

[16] A. S. Vasenko, S. Kawabata, A. A. Golubov, M. Yu. Kupriyanov, C. Lacroix, F. S. Bergeret, and F. W. J. Hekking, Phys. Rev. B **84**, 024524 (2011).

[17] J. S. Jiang, D. Davidovic, D. H. Reich, and C. L. Chien, Phys. Rev. Lett. **74**, 314 (1995).

[18] L. R. Tagirov, Physica C **307**, 145 (1998).

[19] Yu. N. Proshin, Yu. A. Izyumov, and M. G. Khusainov, Phys. Rev. B **64**, 064522 (2001).

[20] Yu. N. Khaydukov, A. S. Vasenko, E. A. Kravtsov, V. V. Progliado, V. D. Zhaketov, A. Csik, Yu. V. Nikitenko, A. V. Petrenko, T. Keller, A. A. Golubov, M. Yu. Kupriyanov, V. V. Ustinov, V. L. Aksenov, and B. Keimer, Phys. Rev. B **97**, 144511 (2018).

[21] T. Karabassov, V. S. Stolyarov, A. A. Golubov, V. M. Silkin, V. M. Bayazitov, B. G. Lvov, and A. S. Vasenko, Phys. Rev. B **100**, 104502 (2019).

[22] L. Fu, C. L. Kane, and E. J. Mele, Phys. Rev. Lett. **98**, 106803 (2007).

[23] M. Z. Hasan and C. L. Kane, Rev. Mod. Phys. **82**, 3045 (2010).

[24] M. Sato and Y. Ando, Rep. Prog. Phys. **80**, 076501 (2017).

[25] S.-Q. Shen, *Topological Insulators Dirac Equation in Condensed Matters* (Springer, Berlin, 2012).

[26] G. Tkachov, *Topological Insulators: The Physics of Spin Helicity in Quantum Transport* (Pan Stanford, Singapore, 2015).

[27] Y. Tanaka, M. Sato, and N. Nagaosa, J. Phys. Soc. Jpn. **81**, 011013 (2012).

[28] S. D. Sarma, M. Freedman, and C. Nayak, Phys. Today **59**(7), 32 (2006).

[29] R. Aguado and L. P. Kouwenhoven, Phys. Today **73**(6), 44 (2020).

[30] X.-L. Qi and S.-C. Zhang, Rev. Mod. Phys. **83**, 1057 (2011).

[31] L. Fu and C. L. Kane, Phys. Rev. Lett. **100**, 096407 (2008).

[32] Y. Tanaka, T. Yokoyama, and N. Nagaosa, Phys. Rev. Lett. **103**, 107002 (2009).

[33] M. Sato and S. Fujimoto, Phys. Rev. B **79**, 094504 (2009).

[34] J. Alicea, Rep. Prog. Phys. **75**, 076501 (2012).

[35] C. W. J. Beenakker, Annu. Rev. Condens. Matter Phys. **4**, 113 (2013).

[36] G. Tkachov and E. M. Hankiewicz, Phys. Rev. B **88**, 075401 (2013).

[37] Y. Lu, P. Virtanen, and T. T. Heikkilä, Phys. Rev. B **102**, 224510 (2020).

[38] A. Yamakage, K. Yada, M. Sato, and Y. Tanaka, Phys. Rev. B **85**, 180509(R) (2012).

[39] B. Lu, K. Yada, A. A. Golubov, and Y. Tanaka, Phys. Rev. B **92**, 100503(R) (2015).

[40] A. M. Black-Schaffer and A. V. Balatsky, Phys. Rev. B **86**, 144506 (2012).

[41] A. M. Black-Schaffer and A. V. Balatsky, Phys. Rev. B **87**, 220506(R) (2013).

[42] G. Tkachov, Phys. Rev. B **87**, 245422 (2013).

[43] P. Burset, B. Lu, G. Tkachov, Y. Tanaka, E. M. Hankiewicz, and B. Trauzettel, Phys. Rev. B **92**, 205424 (2015).

[44] I. V. Bobkova and A. M. Bobkov, Phys. Rev. B **95**, 184518 (2017).

[45] F. S. Bergeret and I. V. Tokatly, Phys. Rev. B **89**, 134517 (2014).

[46] S. H. Jacobsen and J. Linder, Phys. Rev. B **92**, 024501 (2015).

[47] H. G. Hugdal, J. Linder, and S. H. Jacobsen, Phys. Rev. B **95**, 235403 (2017).

[48] B. Bujnowski, R. Biele, and F. S. Bergeret, Phys. Rev. B **100**, 224518 (2019).

[49] J. R. Eskilt, M. Amundsen, N. Banerjee, and J. Linder, Phys. Rev. B **100**, 224519 (2019).

[50] M. Nashaat, I. V. Bobkova, A. M. Bobkov, Y. M. Shukrinov, I. R. Rahmonov, and K. Sengupta, Phys. Rev. B **100**, 054506 (2019).

[51] I. V. Bobkova, A. M. Bobkov, A. A. Zyuzin, and M. Alidoust, Phys. Rev. B **94**, 134506 (2016).

[52] M. Alidoust, Phys. Rev. B **98**, 245418 (2018).

[53] M. Alidoust, Phys. Rev. B **101**, 155123 (2020).

[54] Y. Lu and T. T. Heikkilä, Phys. Rev. B **100**, 104514 (2019).

[55] M. Alidoust and H. Hamzehpour, Phys. Rev. B **96**, 165422 (2017).

[56] A. Zyuzin, M. Alidoust, and D. Loss, Phys. Rev. B **93**, 214502 (2016).

[57] T. Champel and M. Eschrig, Phys. Rev. B **71**, 220506(R) (2005).

[58] T. Champel and M. Eschrig, Phys. Rev. B **72**, 054523 (2005).

[59] T. Champel, T. Löfwander, and M. Eschrig, Phys. Rev. Lett. **100**, 077003 (2008).

[60] N. G. Pugach, M. Safonchik, T. Champel, M. E. Zhitomirsky, E. Lähderanta, M. Eschrig, and C. Lacroix, Appl. Phys. Lett. **111**, 162601 (2017).

[61] N. G. Pugach and M. O. Safonchik, JETP Lett. **107**, 302 (2018).

[62] N. G. Pugach, M. O. Safonchik, D. M. Heim, and V. O. Yagovtsev, Phys. Solid State **60**, 2237 (2018).

[63] M. Bode, M. Heide, K. Von Bergmann, P. Ferriani, S. Heinze, G. Bihlmayer, A. Kubetzka, O. Pietzsch, S. Blügel, and R. Wiesendanger, Nature (London) **447**, 190 (2007).

[64] C. Brun, T. Cren, and D. Roditchev, Supercond. Sci. Technol. **30**, 013003 (2017).

[65] A. S. Vasenko and F. W. J. Hekking, J. Low Temp. Phys. **154**, 221 (2009).

[66] W. Belzig, F. K. Wilhelm, C. Bruder, G. Schön, and A. D. Zaikin, Superlattices Microstruct. **25**, 1251 (1999).

[67] K. D. Usadel, Phys. Rev. Lett. **25**, 507 (1970).

[68] M. Yu. Kupriyanov and V. F. Lukichev, Zh. Eksp. Teor. Fiz. **94**, 139 (1988) [JETP **67**, 1163 (1988)].

[69] E. V. Bezuglyi, A. S. Vasenko, V. S. Shumeiko, and G. Wendin, Phys. Rev. B **72**, 014501 (2005); E. V. Bezuglyi, A. S. Vasenko, E. N. Bratus, V. S. Shumeiko, and G. Wendin, *ibid.* **73**, 220506(R) (2006).